

Precise Measurement of the Λ Electric Dipole Moment through the Entangled Strange Baryon-Antibaryon System

BESIII Collaboration ^{*†}

The dominance of matter over antimatter in the universe has consistently driven the pursuit of new physics beyond the Standard Model that violates charge-parity symmetry. Unlike the well-constrained electrons and neutrons, strange baryons (hyperons) remain a largely unexplored territory, in which interactions between hyperons and particles from new physics could induce a non-trivial electric dipole moment (EDM). However, direct measurements of hyperon EDMs through spin precession are highly challenging due to their short lifetimes. In this paper, we present a novel method to extract the EDM of the lightest hyperon, Λ , using the entangled $\Lambda\bar{\Lambda}$ system. Our result is consistent with zero, achieving a three-order-of-magnitude improvement over the previous upper limit established in the 1980s with comparable statistics, providing stringent constraints on potential new physics.

The existence of a non-zero electric dipole moment (EDM) in a particle signals the violation of time-reversal (T) symmetry and, consequently, charge-parity (CP) symmetry, assuming CPT symmetry holds. The amount of CP violation (CPV) in the Standard Model (SM), arising from a complex phase in the quark mixing matrix and the Quantum Chromodynamic (QCD) vacuum angle $\bar{\theta}$, is insufficient to explain the matter-dominated universe (1, 2). The measurement of EDMs, which are highly

^{*}Collaboration authors and affiliations are listed in the Supplementary Material

[†]These authors contributed equally to this work

sensitive probes for physics beyond the Standard Model (BSM) in the multi- 10^{14} electron-volt mass range, has been conducted across a wide variety of particles, atoms, and molecules (3, 4). However, no EDM or BSM signal has been observed experimentally to date. Systematic searches in baryon systems could provide insights into the QCD vacuum and, in conjunction with leptons (5–7), are essential for uncovering BSM physics (3). An unexpectedly large EDM resulting from interactions between strange quarks in hyperons and new particles could indicate specific types of BSM physics. To achieve a comprehensive understanding of the fundamental laws of physics, a global analysis of EDM searches across various systems—simultaneously constraining the parameters of a general theory integrating SM and BSM physics—requires experimental input from hyperons (4, 8).

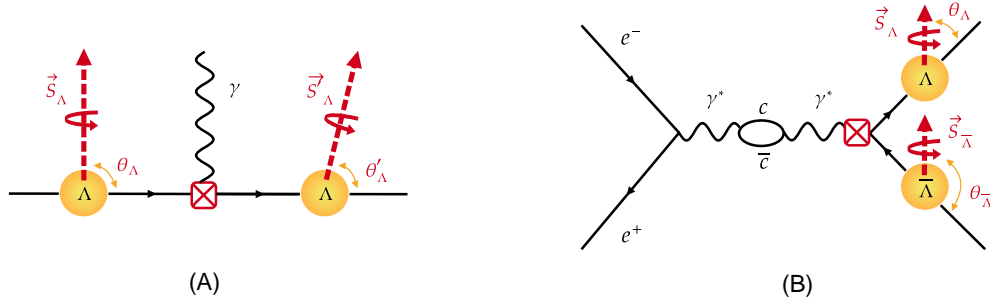


Figure 1: Schematic view of EDM measurements: (A) Determination via spin precession induced by an external electromagnetic field. Here, \vec{S}_Λ and \vec{S}'_Λ denote the spin directions of the Λ particle before and after precession, while θ_Λ and θ'_Λ represent the angles between the spin and momentum directions before and after precession. (B) Definition through a CP-violating form factor via virtual photon exchange between the J/ψ , composed of a charm-anticharm quark pair, and the polarized, spin-entangled $\Lambda\bar{\Lambda}$ system. Here, \vec{S}_Λ and $\vec{S}_{\bar{\Lambda}}$ are the spin directions of the Λ and $\bar{\Lambda}$, respectively, while θ_Λ and $\theta_{\bar{\Lambda}}$ represent the angles between their spin and momentum directions. The \boxtimes symbol indicates a CP-violating interaction vertex.

Experimental overview

The interaction between the spin of a hyperon and an external electromagnetic field induces a precession effect, which can be used to directly measure the hyperon's EDM (Fig. 1A). This approach has been widely employed for EDM measurements of electrons, neutrons, and protons

but remains challenging for short-lived particles such as hyperons. In addition to their short lifetime, producing a well-polarized particle source is difficult. To date, the Λ is the only hyperon whose EDM has been measured. Apart from a few experimental proposals (9, 10), no other EDM measurements have been conducted in the hyperon sector. The most stringent upper limit on the Λ hyperon EDM, $1.5 \times 10^{-16} e \text{ cm}$, was established in 1981 at Fermilab (11). This study also highlighted several challenges that limited further improvements in sensitivity. While increasing the signal yield, optimizing the Λ polarization, and extending the effective magnetic field coverage could enhance precision, reaching $10^{-18} e \text{ cm}$ remains a formidable challenge.

Here, we present an alternative approach in which the spin-entangled $\Lambda\bar{\Lambda}$ pair is produced via the process $e^+e^- \rightarrow J/\psi \rightarrow \Lambda\bar{\Lambda}$. The subtle difference between the angular distributions of the Λ and $\bar{\Lambda}$ can be used to access the Λ EDM. The interaction between the J/ψ and the $\Lambda\bar{\Lambda}$ pair involves the strong force, quantum electrodynamics, and the weak force within the SM. The dominant contribution comes from non-perturbative QCD. Since the Λ is not a point-like particle, its internal structure and the aforementioned interactions are encapsulated in form factors, which depend on the production energy of the $\Lambda\bar{\Lambda}$ pair ($q = m_{J/\psi}$). The violation of parity and CP symmetry in $\Lambda\bar{\Lambda}$ pair production is characterized by the form factors F_A and H_T , respectively, and can originate from various sources. As noted in (12, 13), the contribution from the Λ EDM is assumed to be the dominant source of the CP-violating form factor H_T , mediated by virtual photon exchange between the J/ψ and the $\Lambda\bar{\Lambda}$ pair. The form factor H_T can be related to the Λ EDM (d_Λ) while neglecting its dependence on the production energy,

$$H_T = \frac{2e}{3m_{J/\psi}^2} g_V d_\Lambda. \quad (1)$$

Here, e denotes the magnitude of the electron charge, g_V is determined from the measured branching fraction of $J/\psi \rightarrow e^+e^-$ (12), and $m_{J/\psi}$ represents the mass of J/ψ . Parity symmetry is violated in both the production and decay of the J/ψ meson due to weak force contributions. In the production process, the weak interaction in electron-positron annihilation induces a small longitudinal polarization, P_L . The polarization P_L and the parity-violating form factor F_A are predicted to be of the order of $\mathcal{O}(10^{-4})$ and $\mathcal{O}(10^{-6})$, respectively (14, 15).

The extraction of d_Λ through the CP-violating form factor H_T in $J/\psi \rightarrow \Lambda\bar{\Lambda}$ decays was first proposed in (12, 13). In this paper, we implement this idea using a novel approach (16) in the

process of $e^+e^- \rightarrow J/\psi \rightarrow \Lambda\bar{\Lambda}$ with $\Lambda(\bar{\Lambda})$ decays to proton p (antiproton \bar{p}) and charged pion π^- (π^+) at the BESIII experiment. This approach utilizes the differential decay probability, derived from the full angular distributions of the production and decay of the spin-entangled $\Lambda\bar{\Lambda}$ system. The entanglement, arising from angular momentum conservation, enables a highly sensitive probe of the EDM.

We select three million high-purity $\Lambda\bar{\Lambda}$ pairs from a dataset of 10 billion J/ψ events collected at BESIII in 2009, 2012 and 2017-2019 (17). The signal events are selected through a stringent procedure: Charged particle tracks are reconstructed in the main drift chamber, where a superconducting solenoid generates a magnetic field that enables precise momentum measurement, achieving an accuracy of 0.5% at 1.0 GeV/c. Protons and charged pions are identified based on their momentum information, with high-momentum tracks classified as proton candidates and low-momentum tracks as pion candidates. The $\Lambda(\bar{\Lambda})$ candidates are formed using $p\pi^-$ ($\bar{p}\pi^+$) pairs, with a vertex fit ensuring a common decay position. Their masses are required to fall within the Λ mass window. A kinematic fit imposing energy-momentum conservation constraint improves the momentum resolution of the final-state particles. After applying selection criteria, the final dataset consists of 3,049,187 signal candidates with a purity of 99.9%. For each event, we compute a complete set of kinematic variables, denoted as $\xi = (\theta_\Lambda, \theta_p, \theta_{\bar{p}}, \phi_p, \phi_{\bar{p}})$, using the momenta of both intermediate and final-state particles. Here, θ_Λ represents the angle between the Λ hyperon and the electron beam in the center-of-momentum system of e^+e^- , while θ_p and ϕ_p ($\theta_{\bar{p}}$ and $\phi_{\bar{p}}$) correspond to the polar and azimuthal angles of the proton (antiproton) in the rest frame of the Λ ($\bar{\Lambda}$). We then construct the likelihood function using the differential decay probability of $e^+e^- \rightarrow J/\psi \rightarrow \Lambda(\rightarrow p\pi^-)\bar{\Lambda}(\rightarrow \bar{p}\pi^+)$ as a function of ξ given by Eq. S1 in (18). The longitudinal polarization P_L , form factors F_A and H_T , along with other parameters which are defined in (18), are extracted by minimizing the negative log-likelihood function, accounting for both data and background contribution. During data analysis, the value of parameters P_L , F_A and H_T are blinded by introducing unknown offsets, which were not removed until the event selection, fitting procedure, and systematic uncertainty estimation were fully completed. A comprehensive description of the above procedure is provided in (18).

Table 1: Summary of fitted parameters. The extracted parameters include the J/ψ polarization P_L , which characterizes parity violation in J/ψ production, as well as the form factors F_A and H_T , which represent parity and CP violation in J/ψ decay, respectively. The Λ electric dipole moment (d_Λ) is derived from the fitted value of H_T . The first uncertainty represents the statistical uncertainty, while the second corresponds to the systematic uncertainty.

Parameter	Fitting results
P_L	$(-1.8 \pm 1.2 \pm 0.8) \times 10^{-3}$
$Re(F_A)$	$(-2.4 \pm 1.6 \pm 3.1) \times 10^{-6}$
$Im(F_A)$	$(-7.9 \pm 3.7 \pm 2.5) \times 10^{-6}$
$Re(H_T)$	$(-1.4 \pm 1.4 \pm 0.2) \times 10^{-6} \text{ GeV}^{-1}$
$Im(H_T)$	$(1.3 \pm 1.2 \pm 0.4) \times 10^{-6} \text{ GeV}^{-1}$
$Re(d_\Lambda)$	$(-3.1 \pm 3.2 \pm 0.5) \times 10^{-19} e \text{ cm}$
$Im(d_\Lambda)$	$(2.9 \pm 2.6 \pm 0.6) \times 10^{-19} e \text{ cm}$

Systematic uncertainty evaluation

The major sources of systematic uncertainties of this measurement include background estimation, charged particle reconstruction, vertex reconstruction for $\Lambda(\bar{\Lambda})$, energy-momentum conservation constraints and detector resolution. A comprehensive summary of these uncertainties is provided in Table S1, and detailed information on the systematic uncertainty study can be found in (18). The uncertainties from background estimation and charged particle reconstruction are found to be negligible. The systematic uncertainties related to the Λ and $\bar{\Lambda}$ vertex reconstruction and energy-momentum conservation constraints are assessed using a data-driven method to correct the simulated data. The differences between the measurements with and without efficiency corrections are taken as the systematic uncertainty. The systematic uncertainty arising from detector resolution is evaluated using simulated data resampling according to the differential angular probability shown in Equation S1. The discrepancy between the fitted and the generated values is taken as the systematic uncertainty.

To further evaluate the accuracy of our measurement, we systematically investigated potential

sources of shifts in the EDM, including imperfections in the simulated data and maximum likelihood estimator, as well as $\Lambda(\bar{\Lambda})$ decay vertex reconstruction and corrections for final-state radiation (FSR) (19). The channel of $J/\psi \rightarrow p\pi^-\bar{p}\pi^+$ provides reliable efficiency for charged particle reconstruction and allows us to apply corrections to the simulated data. A set of pseudo-experiments was generated under the null EDM hypothesis to evaluate the behavior of the maximum likelihood estimator. The distribution of the difference between the fitted results from the pseudo-experiments and the null EDM hypothesis is consistent with a normal distribution, and no shift in the EDM was observed. Additionally, we examined whether the reconstruction of the $\Lambda(\bar{\Lambda})$ decay vertex could introduce a potential shift. The data sample was split into several groups according to the $\Lambda(\bar{\Lambda})$ decay length to evaluate the consistency of the measurements, and no shift was observed. The effect of FSR is estimated using simulated data by comparing measurements with and without FSR consideration and is found to be negligible.

EDM results

The results of the fitted parameters are summarized in Table 1. The measurements of the longitudinal polarization of the J/ψ resonance P_L and parity-violating form factor F_A approach the theoretical prediction limits (15). The measurement of the Λ EDM is consistent with zero, preserving CP symmetry with a precision of 10^{-19} e cm,

$$\begin{aligned} Re(d_\Lambda) &= (-3.1 \pm 3.2 \pm 0.5) \times 10^{-19} \text{ e cm}, \\ Im(d_\Lambda) &= (2.9 \pm 2.6 \pm 0.6) \times 10^{-19} \text{ e cm}. \end{aligned} \tag{2}$$

The upper limit of Λ EDM is determined using the MINOS method implemented via the MINUIT algorithm (20), employing a likelihood scan procedure. The corresponding 95% confidence level intervals are:

$$\begin{aligned} -8.6 \times 10^{-19} &< Re(d_\Lambda) < 3.3 \times 10^{-19} \text{ e cm}, \\ -2.5 \times 10^{-19} &< Im(d_\Lambda) < 7.2 \times 10^{-19} \text{ e cm}, \end{aligned} \tag{3}$$

which corresponds to an upper bound of

$$|d_\Lambda| < 6.5 \times 10^{-19} \text{ e cm}. \tag{4}$$

The EDM effect, which refers to the difference in the angular distribution between the entangled Λ and $\bar{\Lambda}$, can be visualized through the projection of the triple-product asymmetry (TPA), $O \equiv$

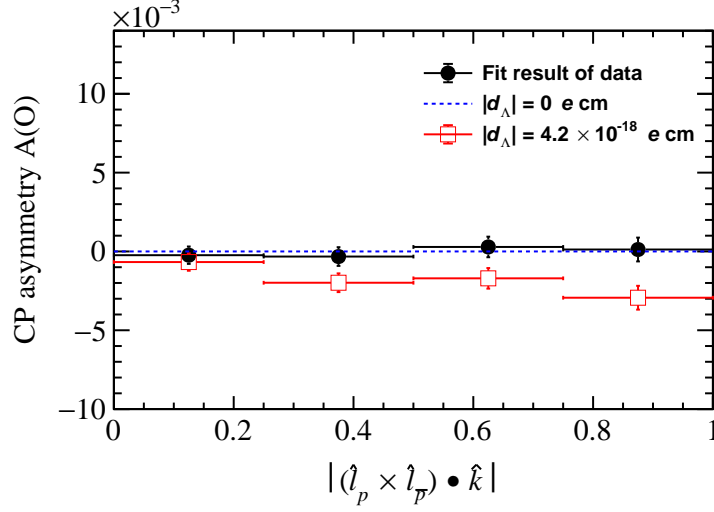


Figure 2: Visualization of the EDM effects. The black data points represent the projection based on the nominal fit to the data, where H_T is consistent with zero within uncertainties. The red data points correspond to the projection under a scenario with a significant non-zero EDM, where H_T deviates from zero by 10 standard deviations, corresponding to $|d_\Lambda| = 4.2 \times 10^{-18} e \text{ cm}$. The blue dashed line shows the projection assuming a strict zero EDM.

$(\hat{l}_p \times \hat{l}_{\bar{p}}) \cdot \hat{k}$, which is proportional to the real part of the form factor H_T (14, 15). Here, $\hat{l}_p(\hat{l}_{\bar{p}})$ and \hat{k} represent the unit momentum of the proton(antiproton) in the rest frame of the $\Lambda(\bar{\Lambda})$ and the unit momentum of Λ in the center-of-mass frame of the e^+e^- system, respectively. The visualization of the effect of EDM is performed by projecting the difference between the positive and negative values of TPA, $A(O) = \frac{N_{\text{event}}(O>0) - N_{\text{event}}(O<0)}{N_{\text{event}}(O>0) + N_{\text{event}}(O<0)}$. This projection is calculated in the regions of the folded TPA using simulated data resampled from the nominal model, corresponding to the fit result of the data. To illustrate the impact of a non-zero EDM, which may be allowed in certain BSM models, we also consider an alternative scenario where H_T deviates from zero by 10 standard deviations, corresponding to $|d_\Lambda| = 4.2 \times 10^{-18} e \text{ cm}$. The EDM visualization for both scenarios is shown in Fig. 2, highlighting the differences between the measurement in this analysis and the non-zero EDM scenario.

Discussion

Our result for the Λ EDM represents a three-order-of-magnitude improvement compared to the latest measurement using data from Fermilab reported in 1981 (11), providing a stringent constraint on various BSM physics models that propose new sources of CPV to resolve the mystery of the matter-dominated universe. The effective Lagrangian (4) describing the EDM interactions is given by

$$L = -\frac{\alpha_s}{8\pi}\bar{\theta}\text{Tr}[G^{\mu\nu}\tilde{G}_{\mu\nu}] - \frac{i}{2}\sum_q d_q\bar{q}F_{\mu\nu}\sigma^{\mu\nu}\gamma^5 q - \frac{i}{2}\sum_q \tilde{d}_q\bar{q}G_{\mu\nu}^a T^a\sigma^{\mu\nu}\gamma^5 q, \quad (5)$$

which encodes the contributions to CP violation and EDMs in the SM and beyond. Here, α_s is the strong coupling constant, $F_{\mu\nu}$ and $G_{\mu\nu} = G_{\mu\nu}^a T^a$ represent the strength of electromagnetic and gluonic fields, respectively. The parameters d_q and \tilde{d}_q correspond to the EDM and chromo-EDM (cEDM) of the quarks, respectively, with the latter arising from CP-violating interactions between the quarks and gluons. The parameters in Equation 5 should be constrained from the measurements of EDM in different systems. In the valence quark model, neglecting contributions from sea quarks, the Λ EDM is related to strange quark EDM as $d_\Lambda = d_s$ (21). When incorporating the contribution from the QCD vacuum angle θ (22), this can be expressed as

$$d_\Lambda = (-2.6 \pm 0.4) \times 10^{-16} \bar{\theta} e \text{ cm} + d_s. \quad (6)$$

On the other hand, the neutron EDM, d_n , is given by lattice QCD (LQCD) as (23, 24)

$$d_n = -(1.5 \pm 0.7) \times 10^{-16} \bar{\theta} e \text{ cm} \\ - (0.20 \pm 0.01)d_u + (0.78 \pm 0.03)d_d + (0.0027 \pm 0.016)d_s \quad (7)$$

Since the contribution of quark cEDMs remains under investigation by several LQCD groups (21), we do not include these contributions in the present analysis. As seen from Equations 6 and 7, the measurement of the EDM for a single hadron is insufficient to disentangle the various potential sources of CP violation in the quark sector. Besides the neutron EDM, the hyperon EDM provides valuable insight into the study of the strange quark EDM. However, it is still insufficient to independently extract constraints on new physics models. In this work, the measurement further constrains the fundamental parameter space. Alongside the upper limit on the neutron EDM, $|d_n| < 1.8 \times 10^{-26} e \text{ cm}$ (25), two scenarios are explored. First, a new physics model incorporating

$SU(3)$ flavor symmetry—which indicates that the u , d , and s quarks behave similarly under strong interactions—is considered, implying $d_u = d_d = d_s$. In contrast, since $m_s > m_u \sim m_d$, a second scenario explores a model without $SU(3)$ flavor symmetry where $d_s \gg d_u, d_d$. Thus, the contributions of the u and d quarks can be neglected. The exclusion for the parameters $\bar{\theta}$ and d_s in these two scenarios are illustrated in Fig. 3, where the first scenario with $SU(3)$ flavor symmetry provides a more stringent constraint.

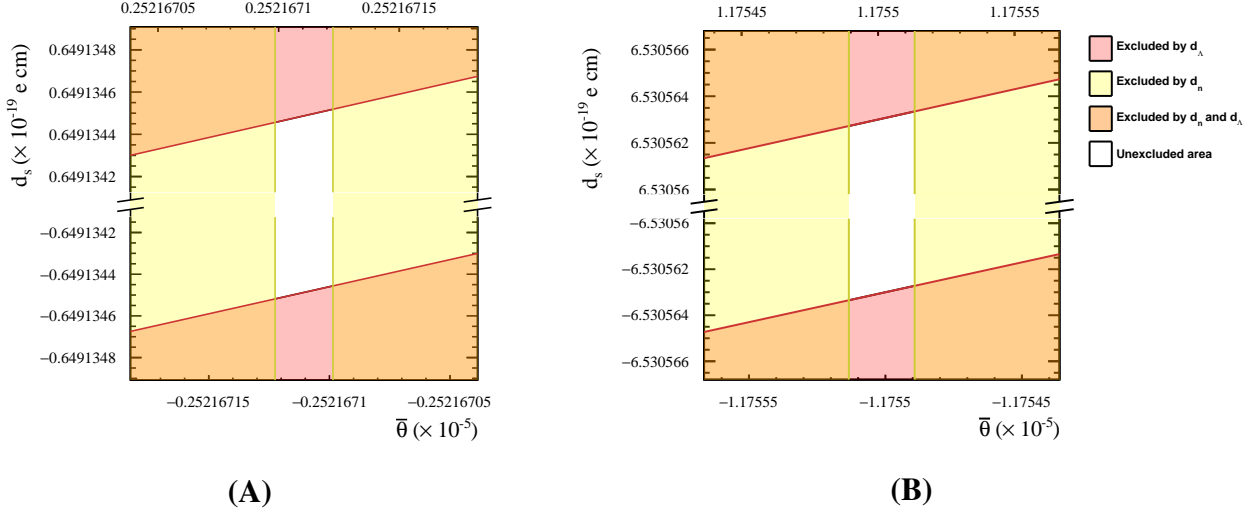


Figure 3: Constraints on parameter space of $\bar{\theta}$ and d_s in two scenarios. (A) and (B) are for scenarios with and without $SU(3)$ flavor symmetry, respectively. For clarity, breaks are introduced in the X and Y axes due to their large disparity. The pink region denotes the parameter space excluded by Λ EDM measurements, the yellow by neutron EDM measurements, and the orange by their combined constraints. The unshaded region denotes the parameter space that remains unconstrained.

In conclusion, a full angular analysis of the $J/\psi \rightarrow \Lambda \bar{\Lambda}$ decay is performed using approximately 3 million signal candidates selected from a sample of 10 billion J/ψ data collected by the BESIII experiment. The entangled $\Lambda \bar{\Lambda}$ system from the J/ψ resonance enhances the sensitivity of angular distributions to the subtle effects from the EDM. The EDM of Λ is simultaneously determined to be an unprecedented precision level of $10^{-19} e \text{ cm}$, representing a three-order-of-magnitude enhancement over the previous result measured 40 years ago with similar statistics (11). Our result, together with the upper limit on the neutron EDM, provides more stringent constraints on the new physics parameter space. This novel method applied for the Λ EDM measurement can be utilized for

the systematic study of the hyperon family in the BESIII experiment. Estimations using simulated data show that a similar measurement precision can be achieved for the Ξ and Σ hyperons (16).

References and Notes

1. A. D. Sakharov. *Pisma Zh. Eksp. Teor. Fiz.* **5**, 32–35 (1967).
2. A. Riotto, Theories of baryogenesis, in *ICTP Summer School in High-Energy Physics and Cosmology* (1998), pp. 326–436.
3. J. Beacham *et al.* *J. Phys. G* **47** (1), 010501 (2020).
4. T. Chupp, P. Fierlinger, M. Ramsey-Musolf, J. Singh. *Rev. Mod. Phys.* **91** (1), 015001 (2019).
5. ACME Collaboration. *Science* **343**, 269–272 (2014).
6. ACME Collaboration. *Nature* **562** (7727), 355–360 (2018).
7. T. S. Roussy *et al.* *Science* **381** (6653), adg4084 (2023).
8. M. Pospelov, A. Ritz. *Annals Phys.* **318**, 119–169 (2005).
9. F. J. Botella *et al.* *Eur. Phys. J. C* **77** (3), 181 (2017).
10. E. Bagli *et al.* *Eur. Phys. J. C* **77** (12), 828 (2017), [Erratum: *Eur.Phys.J.C* 80, 680 (2020)].
11. L. Pondrom *et al.* *Phys. Rev. D* **23**, 814–816 (1981).
12. X.-G. He, J. P. Ma, B. McKellar. *Phys. Rev. D* **47**, R1744–R1746 (1993).
13. X.-G. He, J. P. Ma, B. McKellar. *Phys. Rev. D* **49**, 4548–4552 (1994).
14. X. G. He, J. P. Ma. *Phys. Lett. B* **839**, 137834 (2023).
15. Y. Du, X.-G. He, J.-P. Ma, X.-Y. Du. *Phys. Rev. D* **110** (7), 076019 (2024).
16. J. Fu, H.-B. Li, J.-P. Wang, F.-S. Yu, J. Zhang. *Phys. Rev. D* **108** (9), L091301 (2023).
17. BESIII Collaboration. *Chin. Phys. C* **46** (7), 074001 (2022).
18. Materials and methods are available as supplementary material.
19. E. Richter-Was. *Phys. Lett. B* **303**, 163–169 (1993).

20. W. Verkerke, D. P. Kirkby. *eConf* **C0303241**, MOLT007 (2003).
21. SymLat Collaboration. *Phys. Rev. D* **104** (7), 074516 (2021).
22. F.-K. Guo, U.-G. Meissner. *JHEP* **12**, 097 (2012).
23. J. Dragos, T. Luu, A. Shindler, J. de Vries, A. Yousif. *Phys. Rev. C* **103** (1), 015202 (2021).
24. R. Gupta *et al.* *Phys. Rev. D* **98** (9), 091501 (2018).
25. C. Abel *et al.* *Phys. Rev. Lett.* **124** (8), 081803 (2020).
26. BESIII Collaboration. *Nucl. Instrum. Meth. A* **614**, 345–399 (2010).
27. BESIII Collaboration. *Chin. Phys. C* **44** (4), 040001 (2020).
28. S. Agostinelli *et al.* *Nucl. Instrum. Meth. A* **506**, 250–303 (2003).
29. Z.-Y. Deng *et al.* *Chin. Phys. C* **30**, 371 (2006).
30. S. Jadach, B. F. L. Ward, Z. Was. *Phys. Rev. D* **63**, 113009 (2001).
31. R.-G. Ping. *Chin. Phys. C* **32**, 599 (2008).
32. J. C. Chen, G. S. Huang, X. R. Qi, D. H. Zhang, Y. S. Zhu. *Phys. Rev. D* **62**, 034003 (2000).
33. R.-L. Yang, R.-G. Ping, H. Chen. *Chin. Phys. Lett.* **31**, 061301 (2014).
34. BESIII Collaboration. *Nature Phys.* **15**, 631–634 (2019).
35. BESIII Collaboration. *Phys. Rev. Lett.* **129** (13), 131801 (2022).
36. S. Navas *et al.* (Particle Data Group). *Phys. Rev. D* **110** (3), 030001 (2024).
37. T. D. Lee, C.-N. Yang. *Phys. Rev.* **108**, 1645–1647 (1957).

Acknowledgments

The BESIII Collaboration thanks the staff of BEPCII (<https://cstr.cn/31109.02.BEPC>) and the IHEP computing center for their strong support. This work is supported in part by National Key R&D Program of China under Contracts Nos. 2023YFA1606000, 2020YFA0406300, 2020YFA0406400, 2023YFA1606704; National Natural Science Foundation of China (NSFC) under Contracts Nos. 11635010, 11935015, 11935016, 11935018, 12025502, 12035009, 12035013, 12061131003, 12192260, 12192261, 12192262, 12192263, 12192264, 12192265, 12221005, 12225509, 12235017, 12275058, 12361141819, 12475082; the Chinese Academy of Sciences (CAS) Large-Scale Scientific Facility Program; CAS under Contract No. YSBR-101; 100 Talents Program of CAS; The Institute of Nuclear and Particle Physics (INPAC) and Shanghai Key Laboratory for Particle Physics and Cosmology; the Natural Science Foundation of Shan-dong Province under Contract No. ZR2023MA004; German Research Foundation DFG under Contract No. FOR5327; Istituto Nazionale di Fisica Nucleare, Italy; Knut and Alice Wallenberg Foundation under Contracts Nos. 2021.0174, 2021.0299; Ministry of Development of Turkey under Contract No. DPT2006K-120470; National Research Foundation of Korea under Contract No. NRF-2022R1A2C1092335; National Science and Technology fund of Mongolia; National Science Research and Innovation Fund (NSRF) via the Program Management Unit for Human Resources & Institutional Development, Research and Innovation of Thailand under Contract No. B50G670107; Polish National Science Centre under Contract No. 2024/53/B/ST2/00975; Swedish Research Council under Contract No. 2019.04595; U. S. Department of Energy under Contract No. DE-FG02-05ER41374.

Author contributions: All authors have contributed to the publication, being variously involved in the design and the construction of the detectors, in writing software, calibrating sub-systems, operating the detectors and acquiring data and finally analysing the processed data.

Competing interests: The authors declare no competing interests.

Supplementary materials

BESIII Collaboration Author List

Materials and Methods

Fig. S1

Tables S1 and S2

References (26–37)

Supplementary Materials for Precise Measurement of the Λ Electric Dipole Moment through the Entangled Strange Baryon-Antibaryon System

The BESIII Collaboration

This PDF file includes:

BESIII Collaboration Author List

Materials and Methods

Fig. S1

Tables S1 and S2

References (26–37)

BESIII Collaboration authors and affiliations

M. Ablikim¹, M. N. Achasov^{4,c}, P. Adlarson⁷⁷, X. C. Ai⁸², R. Aliberti³⁶, A. Amoroso^{76A,76C}, Q. An^{73,59,a}, Y. Bai⁵⁸, O. Bakina³⁷, Y. Ban^{47,h}, H.-R. Bao⁶⁵, S. S. Bao⁵¹, V. Batozskaya^{1,45}, K. Begzsuren³³, N. Berger³⁶, M. Berlowski⁴⁵, M. Bertani^{29A}, D. Bettoni^{30A}, F. Bianchi^{76A,76C}, E. Bianco^{76A,76C}, A. Bortone^{76A,76C}, I. Boyko³⁷, R. A. Briere⁵, A. Brueggemann⁷⁰, H. Cai⁷⁸, M. H. Cai^{39,k,l}, X. Cai^{1,59}, A. Calcaterra^{29A}, G. F. Cao^{1,65}, N. Cao^{1,65}, S. A. Cetin^{63A}, X. Y. Chai^{47,h}, J. F. Chang^{1,59}, G. R. Che⁴⁴, Y. Z. Che^{1,59,65}, C. H. Chen⁹, Chao Chen⁵⁶, G. Chen¹, H. S. Chen^{1,65}, H. Y. Chen²¹, M. L. Chen^{1,59,65}, S. J. Chen⁴³, S. L. Chen⁴⁶, S. M. Chen⁶², T. Chen^{1,65}, X. R. Chen^{32,65}, X. T. Chen^{1,65}, X. Y. Chen^{12,g}, Y. B. Chen^{1,59}, Y. Q. Chen³⁵, Y. Q. Chen¹⁶, Z. J. Chen^{26,i}, Z. K. Chen⁶⁰, S. K. Choi¹⁰, X. Chu^{12,g}, G. Cibinetto^{30A}, F. Cossio^{76C}, J. Cottee-Meldrum⁶⁴, J. J. Cui⁵¹, H. L. Dai^{1,59}, J. P. Dai⁸⁰, A. Dbeyssi¹⁹, R. E. de Boer³, D. Dedovich³⁷, C. Q. Deng⁷⁴, Z. Y. Deng¹, A. Denig³⁶, I. Denysenko³⁷, M. Destefanis^{76A,76C}, F. De Mori^{76A,76C}, B. Ding^{68,1}, X. X. Ding^{47,h}, Y. Ding³⁵, Y. Ding⁴¹, Y. X. Ding³¹, J. Dong^{1,59}, L. Y. Dong^{1,65}, M. Y. Dong^{1,59,65}, X. Dong⁷⁸, M. C. Du¹, S. X. Du⁸², S. X. Du^{12,g}, Y. Y. Duan⁵⁶, P. Egorov^{37,b}, G. F. Fan⁴³, J. J. Fan²⁰, Y. H. Fan⁴⁶, J. Fang⁶⁰, J. Fang^{1,59}, S. S. Fang^{1,65}, W. X. Fang¹, Y. Q. Fang^{1,59}, R. Farinelli^{30A}, L. Fava^{76B,76C}, F. Feldbauer³, G. Felici^{29A}, C. Q. Feng^{73,59}, J. H. Feng¹⁶, L. Feng^{39,k,l}, Q. X. Feng^{39,k,l}, Y. T. Feng^{73,59}, M. Fritsch³, C. D. Fu¹, J. L. Fu⁶⁵, Y. W. Fu^{1,65}, H. Gao⁶⁵, X. B. Gao⁴², Y. Gao^{73,59}, Y. N. Gao^{47,h}, Y. N. Gao²⁰, Y. Y. Gao³¹, S. Garbolino^{76C}, I. Garzia^{30A,30B}, P. T. Ge²⁰, Z. W. Ge⁴³, C. Geng⁶⁰, E. M. Gersabeck⁶⁹, A. Gilman⁷¹, K. Goetzen¹³, J. D. Gong³⁵, L. Gong⁴¹, W. X. Gong^{1,59}, W. Gradl³⁶, S. Gramigna^{30A,30B}, M. Greco^{76A,76C}, M. H. Gu^{1,59}, Y. T. Gu¹⁵, C. Y. Guan^{1,65}, A. Q. Guo³², L. B. Guo⁴², M. J. Guo⁵¹, R. P. Guo⁵⁰, Y. P. Guo^{12,g}, A. Guskov^{37,b}, J. Gutierrez²⁸, K. L. Han⁶⁵, T. T. Han¹, F. Hanisch³, K. D. Hao^{73,59}, X. Q. Hao²⁰, F. A. Harris⁶⁷, K. K. He⁵⁶, K. L. He^{1,65}, F. H. Heinsius³, C. H. Heinz³⁶, Y. K. Heng^{1,59,65}, C. Herold⁶¹, P. C. Hong³⁵, G. Y. Hou^{1,65}, X. T. Hou^{1,65}, Y. R. Hou⁶⁵, Z. L. Hou¹, H. M. Hu^{1,65}, J. F. Hu^{57,j}, Q. P. Hu^{73,59}, S. L. Hu^{12,g}, T. Hu^{1,59,65}, Y. Hu¹, Z. M. Hu⁶⁰, G. S. Huang^{73,59}, K. X. Huang⁶⁰, L. Q. Huang^{32,65}, P. Huang⁴³, X. T. Huang⁵¹, Y. P. Huang¹, Y. S. Huang⁶⁰, T. Hussain⁷⁵, N. Hüsken³⁶, N. in der Wiesche⁷⁰, J. Jackson²⁸, Q. Ji¹, Q. P. Ji²⁰, W. Ji^{1,65}, X. B. Ji^{1,65}, X. L. Ji^{1,59}, Y. Y. Ji⁵¹, Z. K. Jia^{73,59}, D. Jiang^{1,65}, H. B. Jiang⁷⁸, P. C. Jiang^{47,h}, S. J. Jiang⁹, T. J. Jiang¹⁷, X. S. Jiang^{1,59,65}, Y. Jiang⁶⁵, J. B. Jiao⁵¹, J. K. Jiao³⁵, Z. Jiao²⁴, S. Jin⁴³, Y. Jin⁶⁸, M. Q. Jing^{1,65}, X. M. Jing⁶⁵, T. Johansson⁷⁷,

S. Kabana³⁴, N. Kalantar-Nayestanaki⁶⁶, X. L. Kang⁹, X. S. Kang⁴¹, M. Kavatsyuk⁶⁶, B. C. Ke⁸²,
 V. Khachatryan²⁸, A. Khokkaz⁷⁰, R. Kiuchi¹, O. B. Kolcu^{63A}, B. Kopf³, M. Kuessner³, X. Kui^{1,65},
 N. Kumar²⁷, A. Kupsc^{45,77}, W. Kühn³⁸, Q. Lan⁷⁴, W. N. Lan²⁰, T. T. Lei^{73,59}, M. Lellmann³⁶,
 T. Lenz³⁶, C. Li⁴⁸, C. Li^{73,59}, C. Li⁴⁴, C. H. Li⁴⁰, C. K. Li²¹, D. M. Li⁸², F. Li^{1,59}, G. Li¹, H. B. Li^{1,65},
 H. J. Li²⁰, H. N. Li^{57,j}, Hui Li⁴⁴, J. R. Li⁶², J. S. Li⁶⁰, K. Li¹, K. L. Li²⁰, K. L. Li^{39,k,l}, L. J. Li^{1,65},
 Lei Li⁴⁹, M. H. Li⁴⁴, M. R. Li^{1,65}, P. L. Li⁶⁵, P. R. Li^{39,k,l}, Q. M. Li^{1,65}, Q. X. Li⁵¹, R. Li^{18,32},
 S. X. Li¹², T. Li⁵¹, T. Y. Li⁴⁴, W. D. Li^{1,65}, W. G. Li^{1,a}, X. Li^{1,65}, X. H. Li^{73,59}, X. L. Li⁵¹, X. Y. Li^{1,8},
 X. Z. Li⁶⁰, Y. Li²⁰, Y. G. Li^{47,h}, Y. P. Li³⁵, Z. J. Li⁶⁰, Z. Y. Li⁸⁰, H. Liang^{73,59}, Y. F. Liang⁵⁵,
 Y. T. Liang^{32,65}, G. R. Liao¹⁴, L. B. Liao⁶⁰, M. H. Liao⁶⁰, Y. P. Liao^{1,65}, J. Libby²⁷, A. Limphirat⁶¹,
 C. C. Lin⁵⁶, D. X. Lin^{32,65}, L. Q. Lin⁴⁰, T. Lin¹, B. J. Liu¹, B. X. Liu⁷⁸, C. Liu³⁵, C. X. Liu¹, F. Liu¹,
 F. H. Liu⁵⁴, Feng Liu⁶, G. M. Liu^{57,j}, H. Liu^{39,k,l}, H. B. Liu¹⁵, H. H. Liu¹, H. M. Liu^{1,65}, Hui-
 hui Liu²², J. B. Liu^{73,59}, J. J. Liu²¹, K. Liu^{39,k,l}, K. Liu⁷⁴, K. Y. Liu⁴¹, Ke Liu²³, L. C. Liu⁴⁴, Lu Liu⁴⁴,
 M. H. Liu^{12,g}, P. L. Liu¹, Q. Liu⁶⁵, S. B. Liu^{73,59}, T. Liu^{12,g}, W. K. Liu⁴⁴, W. M. Liu^{73,59}, W. T. Liu⁴⁰,
 X. Liu^{39,k,l}, X. Liu⁴⁰, X. K. Liu^{39,k,l}, X. Y. Liu⁷⁸, Y. Liu⁸², Y. Liu^{39,k,l}, Y. Liu⁸², Y. B. Liu⁴⁴,
 Z. A. Liu^{1,59,65}, Z. D. Liu⁹, Z. Q. Liu⁵¹, X. C. Lou^{1,59,65}, F. X. Lu⁶⁰, H. J. Lu²⁴, J. G. Lu^{1,59},
 X. L. Lu¹⁶, Y. Lu⁷, Y. H. Lu^{1,65}, Y. P. Lu^{1,59}, Z. H. Lu^{1,65}, C. L. Luo⁴², J. R. Luo⁶⁰, J. S. Luo^{1,65},
 M. X. Luo⁸¹, T. Luo^{12,g}, X. L. Luo^{1,59}, Z. Y. Lv²³, X. R. Lyu^{65,p}, Y. F. Lyu⁴⁴, Y. H. Lyu⁸²,
 F. C. Ma⁴¹, H. L. Ma¹, J. L. Ma^{1,65}, L. L. Ma⁵¹, L. R. Ma⁶⁸, Q. M. Ma¹, R. Q. Ma^{1,65}, R. Y. Ma²⁰,
 T. Ma^{73,59}, X. T. Ma^{1,65}, X. Y. Ma^{1,59}, Y. M. Ma³², F. E. Maas¹⁹, I. MacKay⁷¹, M. Maggiora^{76A,76C},
 S. Malde⁷¹, Q. A. Malik⁷⁵, H. X. Mao^{39,k,l}, Y. J. Mao^{47,h}, Z. P. Mao¹, S. Marcello^{76A,76C},
 A. Marshall⁶⁴, F. M. Melendi^{30A,30B}, Y. H. Meng⁶⁵, Z. X. Meng⁶⁸, G. Mezzadri^{30A}, H. Miao^{1,65},
 T. J. Min⁴³, R. E. Mitchell²⁸, X. H. Mo^{1,59,65}, B. Moses²⁸, N. Yu. Muchnoi^{4,c}, J. Muskalla³⁶,
 Y. Nefedov³⁷, F. Nerling^{19,e}, L. S. Nie²¹, I. B. Nikolaev^{4,c}, Z. Ning^{1,59}, S. Nisar^{11,m}, Q. L. Niu^{39,k,l},
 W. D. Niu^{12,g}, C. Normand⁶⁴, S. L. Olsen^{10,65}, Q. Ouyang^{1,59,65}, S. Pacetti^{29B,29C}, X. Pan⁵⁶,
 Y. Pan⁵⁸, A. Pathak¹⁰, Y. P. Pei^{73,59}, M. Pelizaeus³, H. P. Peng^{73,59}, X. J. Peng^{39,k,l}, Y. Y. Peng^{39,k,l},
 K. Peters^{13,e}, K. Petridis⁶⁴, J. L. Ping⁴², R. G. Ping^{1,65}, S. Plura³⁶, V. Prasad³⁵, F. Z. Qi¹,
 H. R. Qi⁶², M. Qi⁴³, S. Qian^{1,59}, W. B. Qian⁶⁵, C. F. Qiao⁶⁵, J. H. Qiao²⁰, J. J. Qin⁷⁴, J. L. Qin⁵⁶,
 L. Q. Qin¹⁴, L. Y. Qin^{73,59}, P. B. Qin⁷⁴, X. P. Qin^{12,g}, X. S. Qin⁵¹, Z. H. Qin^{1,59}, J. F. Qiu¹,
 Z. H. Qu⁷⁴, J. Rademacker⁶⁴, C. F. Redmer³⁶, A. Rivetti^{76C}, M. Rolo^{76C}, G. Rong^{1,65}, S. S. Rong^{1,65},
 F. Rosini^{29B,29C}, Ch. Rosner¹⁹, M. Q. Ruan^{1,59}, N. Salone⁴⁵, A. Sarantsev^{37,d}, Y. Schelhaas³⁶,

K. Schoenning⁷⁷, M. Scodreggio^{30A}, K. Y. Shan^{12,g}, W. Shan²⁵, X. Y. Shan^{73,59}, Z. J. Shang^{39,k,l},
 J. F. Shangguan¹⁷, L. G. Shao^{1,65}, M. Shao^{73,59}, C. P. Shen^{12,g}, H. F. Shen^{1,8}, W. H. Shen⁶⁵,
 X. Y. Shen^{1,65}, B. A. Shi⁶⁵, H. Shi^{73,59}, J. L. Shi^{12,g}, J. Y. Shi¹, S. Y. Shi⁷⁴, X. Shi^{1,59}, H. L. Song^{73,59},
 J. J. Song²⁰, T. Z. Song⁶⁰, W. M. Song³⁵, Y. J. Song^{12,g}, Y. X. Song^{47,h,n}, S. Sosio^{76A,76C},
 S. Spataro^{76A,76C}, F. Stieler³⁶, S. S. Su⁴¹, Y. J. Su⁶⁵, G. B. Sun⁷⁸, G. X. Sun¹, H. Sun⁶⁵, H. K. Sun¹,
 J. F. Sun²⁰, K. Sun⁶², L. Sun⁷⁸, S. S. Sun^{1,65}, T. Sun^{52,f}, Y. C. Sun⁷⁸, Y. H. Sun³¹, Y. J. Sun^{73,59},
 Y. Z. Sun¹, Z. Q. Sun^{1,65}, Z. T. Sun⁵¹, C. J. Tang⁵⁵, G. Y. Tang¹, J. Tang⁶⁰, J. J. Tang^{73,59},
 L. F. Tang⁴⁰, Y. A. Tang⁷⁸, L. Y. Tao⁷⁴, M. Tat⁷¹, J. X. Teng^{73,59}, J. Y. Tian^{73,59}, W. H. Tian⁶⁰,
 Y. Tian³², Z. F. Tian⁷⁸, I. Uman^{63B}, B. Wang⁶⁰, B. Wang¹, Bo Wang^{73,59}, C. Wang^{39,k,l}, C. Wang²⁰,
 Cong Wang²³, D. Y. Wang^{47,h}, H. J. Wang^{39,k,l}, J. J. Wang⁷⁸, K. Wang^{1,59}, L. L. Wang¹, L. W. Wang³⁵,
 M. Wang^{73,59}, M. Wang⁵¹, N. Y. Wang⁶⁵, S. Wang^{12,g}, T. Wang^{12,g}, T. J. Wang⁴⁴, W. Wang⁶⁰,
 W. Wang⁷⁴, W. P. Wang^{36,59,73,o}, X. Wang^{47,h}, X. F. Wang^{39,k,l}, X. J. Wang⁴⁰, X. L. Wang^{12,g},
 X. N. Wang¹, Y. Wang⁶², Y. D. Wang⁴⁶, Y. F. Wang^{1,8,65}, Y. H. Wang^{39,k,l}, Y. J. Wang^{73,59},
 Y. L. Wang²⁰, Y. N. Wang⁷⁸, Y. Q. Wang¹, Yaqian Wang¹⁸, Yi Wang⁶², Yuan Wang^{18,32}, Z. Wang^{1,59},
 Z. L. Wang², Z. L. Wang⁷⁴, Z. Q. Wang^{12,g}, Z. Y. Wang^{1,65}, D. H. Wei¹⁴, H. R. Wei⁴⁴, F. Weidner⁷⁰,
 S. P. Wen¹, Y. R. Wen⁴⁰, U. Wiedner³, G. Wilkinson⁷¹, M. Wolke⁷⁷, C. Wu⁴⁰, J. F. Wu^{1,8}, L. H. Wu¹,
 L. J. Wu^{1,65}, L. J. Wu²⁰, Lianjie Wu²⁰, S. G. Wu^{1,65}, S. M. Wu⁶⁵, X. Wu^{12,g}, X. H. Wu³⁵, Y. J. Wu³²,
 Z. Wu^{1,59}, L. Xia^{73,59}, X. M. Xian⁴⁰, B. H. Xiang^{1,65}, D. Xiao^{39,k,l}, G. Y. Xiao⁴³, H. Xiao⁷⁴, Y.
 L. Xiao^{12,g}, Z. J. Xiao⁴², C. Xie⁴³, K. J. Xie^{1,65}, X. H. Xie^{47,h}, Y. Xie⁵¹, Y. G. Xie^{1,59}, Y. H. Xie⁶,
 Z. P. Xie^{73,59}, T. Y. Xing^{1,65}, C. F. Xu^{1,65}, C. J. Xu⁶⁰, G. F. Xu¹, H. Y. Xu^{68,2}, H. Y. Xu²,
 M. Xu^{73,59}, Q. J. Xu¹⁷, Q. N. Xu³¹, T. D. Xu⁷⁴, W. Xu¹, W. L. Xu⁶⁸, X. P. Xu⁵⁶, Y. Xu⁴¹, Y. Xu^{12,g},
 Y. C. Xu⁷⁹, Z. S. Xu⁶⁵, F. Yan^{12,g}, H. Y. Yan⁴⁰, L. Yan^{12,g}, W. B. Yan^{73,59}, W. C. Yan⁸², W. H. Yan⁶,
 W. P. Yan²⁰, X. Q. Yan^{1,65}, H. J. Yang^{52,f}, H. L. Yang³⁵, H. X. Yang¹, J. H. Yang⁴³, R. J. Yang²⁰,
 T. Yang¹, Y. Yang^{12,g}, Y. F. Yang⁴⁴, Y. H. Yang⁴³, Y. Q. Yang⁹, Y. X. Yang^{1,65}, Y. Z. Yang²⁰,
 M. Ye^{1,59}, M. H. Ye^{8,a}, Z. J. Ye^{57,j}, Junhao Yin⁴⁴, Z. Y. You⁶⁰, B. X. Yu^{1,59,65}, C. X. Yu⁴⁴, G. Yu¹³,
 J. S. Yu^{26,i}, L. Q. Yu^{12,g}, M. C. Yu⁴¹, T. Yu⁷⁴, X. D. Yu^{47,h}, Y. C. Yu⁸², C. Z. Yuan^{1,65}, H. Yuan^{1,65},
 J. Yuan³⁵, J. Yuan⁴⁶, L. Yuan², S. C. Yuan^{1,65}, X. Q. Yuan¹, Y. Yuan^{1,65}, Z. Y. Yuan⁶⁰, C. X. Yue⁴⁰,
 Ying Yue²⁰, A. A. Zafar⁷⁵, S. H. Zeng^{64A,64B,64C,64D}, X. Zeng^{12,g}, Y. Zeng^{26,i}, Y. J. Zeng⁶⁰,
 Y. J. Zeng^{1,65}, X. Y. Zhai³⁵, Y. H. Zhan⁶⁰, A. Q. Zhang^{1,65}, B. L. Zhang^{1,65}, B. X. Zhang¹,
 D. H. Zhang⁴⁴, G. Y. Zhang^{1,65}, G. Y. Zhang²⁰, H. Zhang^{73,59}, H. Zhang⁸², H. C. Zhang^{1,59,65},

H. H. Zhang⁶⁰, H. Q. Zhang^{1,59,65}, H. R. Zhang^{73,59}, H. Y. Zhang^{1,59}, J. Zhang⁶⁰, J. Zhang⁸², J. J. Zhang⁵³, J. L. Zhang²¹, J. Q. Zhang⁴², J. S. Zhang^{12,g}, J. W. Zhang^{1,59,65}, J. X. Zhang^{39,k,l}, J. Y. Zhang¹, J. Z. Zhang^{1,65}, Jianyu Zhang⁶⁵, L. M. Zhang⁶², Lei Zhang⁴³, N. Zhang⁸², P. Zhang^{1,8}, Q. Zhang²⁰, Q. Y. Zhang³⁵, R. Y. Zhang^{39,k,l}, S. H. Zhang^{1,65}, Shulei Zhang^{26,i}, X. M. Zhang¹, X. Y. Zhang⁴¹, X. Y. Zhang⁵¹, Y. Zhang⁷⁴, Y. Zhang¹, Y. T. Zhang⁸², Y. H. Zhang^{1,59}, Y. M. Zhang⁴⁰, Y. P. Zhang^{73,59}, Z. D. Zhang¹, Z. H. Zhang¹, Z. L. Zhang³⁵, Z. L. Zhang⁵⁶, Z. X. Zhang²⁰, Z. Y. Zhang⁷⁸, Z. Y. Zhang⁴⁴, Z. Z. Zhang⁴⁶, Zh. Zh. Zhang²⁰, G. Zhao¹, J. Y. Zhao^{1,65}, J. Z. Zhao^{1,59}, L. Zhao^{73,59}, L. Zhao¹, M. G. Zhao⁴⁴, N. Zhao⁸⁰, R. P. Zhao⁶⁵, S. J. Zhao⁸², Y. B. Zhao^{1,59}, Y. L. Zhao⁵⁶, Y. X. Zhao^{32,65}, Z. G. Zhao^{73,59}, A. Zhemchugov^{37,b}, B. Zheng⁷⁴, B. M. Zheng³⁵, J. P. Zheng^{1,59}, W. J. Zheng^{1,65}, X. R. Zheng²⁰, Y. H. Zheng^{65,p}, B. Zhong⁴², C. Zhong²⁰, H. Zhou^{36,51,o}, J. Q. Zhou³⁵, J. Y. Zhou³⁵, S. Zhou⁶, X. Zhou⁷⁸, X. K. Zhou⁶, X. R. Zhou^{73,59}, X. Y. Zhou⁴⁰, Y. X. Zhou⁷⁹, Y. Z. Zhou^{12,g}, A. N. Zhu⁶⁵, J. Zhu⁴⁴, K. Zhu¹, K. J. Zhu^{1,59,65}, K. S. Zhu^{12,g}, L. Zhu³⁵, L. X. Zhu⁶⁵, S. H. Zhu⁷², T. J. Zhu^{12,g}, W. D. Zhu^{12,g}, W. D. Zhu⁴², W. J. Zhu¹, W. Z. Zhu²⁰, Y. C. Zhu^{73,59}, Z. A. Zhu^{1,65}, X. Y. Zhuang⁴⁴, J. H. Zou¹, J. Zu^{73,59}

(BESIII Collaboration)

¹ *Institute of High Energy Physics, Beijing 100049, People's Republic of China*

² *Beihang University, Beijing 100191, People's Republic of China*

³ *Bochum Ruhr-University, D-44780 Bochum, Germany*

⁴ *Budker Institute of Nuclear Physics SB RAS (BINP), Novosibirsk 630090, Russia*

⁵ *Carnegie Mellon University, Pittsburgh, Pennsylvania 15213, USA*

⁶ *Central China Normal University, Wuhan 430079, People's Republic of China*

⁷ *Central South University, Changsha 410083, People's Republic of China*

⁸ *China Center of Advanced Science and Technology, Beijing 100190, People's Republic of China*

⁹ *China University of Geosciences, Wuhan 430074, People's Republic of China*

¹⁰ *Chung-Ang University, Seoul, 06974, Republic of Korea*

¹¹ *COMSATS University Islamabad, Lahore Campus, Defence Road, Off Raiwind Road, 54000 Lahore, Pakistan*

¹² *Fudan University, Shanghai 200433, People's Republic of China*

¹³ *GSI Helmholtzcentre for Heavy Ion Research GmbH, D-64291 Darmstadt, Germany*

- ¹⁴ *Guangxi Normal University, Guilin 541004, People's Republic of China*
- ¹⁵ *Guangxi University, Nanning 530004, People's Republic of China*
- ¹⁶ *Guangxi University of Science and Technology, Liuzhou 545006, People's Republic of China*
- ¹⁷ *Hangzhou Normal University, Hangzhou 310036, People's Republic of China*
- ¹⁸ *Hebei University, Baoding 071002, People's Republic of China*
- ¹⁹ *Helmholtz Institute Mainz, Staudinger Weg 18, D-55099 Mainz, Germany*
- ²⁰ *Henan Normal University, Xinxiang 453007, People's Republic of China*
- ²¹ *Henan University, Kaifeng 475004, People's Republic of China*
- ²² *Henan University of Science and Technology, Luoyang 471003, People's Republic of China*
- ²³ *Henan University of Technology, Zhengzhou 450001, People's Republic of China*
- ²⁴ *Huangshan College, Huangshan 245000, People's Republic of China*
- ²⁵ *Hunan Normal University, Changsha 410081, People's Republic of China*
- ²⁶ *Hunan University, Changsha 410082, People's Republic of China*
- ²⁷ *Indian Institute of Technology Madras, Chennai 600036, India*
- ²⁸ *Indiana University, Bloomington, Indiana 47405, USA*
- ²⁹ *INFN Laboratori Nazionali di Frascati , (A)INFN Laboratori Nazionali di Frascati, I-00044, Frascati, Italy; (B)INFN Sezione di Perugia, I-06100, Perugia, Italy; (C)University of Perugia, I-06100, Perugia, Italy*
- ³⁰ *INFN Sezione di Ferrara, (A)INFN Sezione di Ferrara, I-44122, Ferrara, Italy; (B)University of Ferrara, I-44122, Ferrara, Italy*
- ³¹ *Inner Mongolia University, Hohhot 010021, People's Republic of China*
- ³² *Institute of Modern Physics, Lanzhou 730000, People's Republic of China*
- ³³ *Institute of Physics and Technology, Mongolian Academy of Sciences, Peace Avenue 54B, Ulaanbaatar 13330, Mongolia*
- ³⁴ *Instituto de Alta Investigación, Universidad de Tarapacá, Casilla 7D, Arica 1000000, Chile*
- ³⁵ *Jilin University, Changchun 130012, People's Republic of China*
- ³⁶ *Johannes Gutenberg University of Mainz, Johann-Joachim-Becher-Weg 45, D-55099 Mainz, Germany*
- ³⁷ *Joint Institute for Nuclear Research, 141980 Dubna, Moscow region, Russia*
- ³⁸ *Justus-Liebig-Universitaet Giessen, II. Physikalisches Institut, Heinrich-Buff-Ring 16, D-35392*

Giessen, Germany

³⁹ *Lanzhou University, Lanzhou 730000, People's Republic of China*

⁴⁰ *Liaoning Normal University, Dalian 116029, People's Republic of China*

⁴¹ *Liaoning University, Shenyang 110036, People's Republic of China*

⁴² *Nanjing Normal University, Nanjing 210023, People's Republic of China*

⁴³ *Nanjing University, Nanjing 210093, People's Republic of China*

⁴⁴ *Nankai University, Tianjin 300071, People's Republic of China*

⁴⁵ *National Centre for Nuclear Research, Warsaw 02-093, Poland*

⁴⁶ *North China Electric Power University, Beijing 102206, People's Republic of China*

⁴⁷ *Peking University, Beijing 100871, People's Republic of China*

⁴⁸ *Qufu Normal University, Qufu 273165, People's Republic of China*

⁴⁹ *Renmin University of China, Beijing 100872, People's Republic of China*

⁵⁰ *Shandong Normal University, Jinan 250014, People's Republic of China*

⁵¹ *Shandong University, Jinan 250100, People's Republic of China*

⁵² *Shanghai Jiao Tong University, Shanghai 200240, People's Republic of China*

⁵³ *Shanxi Normal University, Linfen 041004, People's Republic of China*

⁵⁴ *Shanxi University, Taiyuan 030006, People's Republic of China*

⁵⁵ *Sichuan University, Chengdu 610064, People's Republic of China*

⁵⁶ *Soochow University, Suzhou 215006, People's Republic of China*

⁵⁷ *South China Normal University, Guangzhou 510006, People's Republic of China*

⁵⁸ *Southeast University, Nanjing 211100, People's Republic of China*

⁵⁹ *State Key Laboratory of Particle Detection and Electronics, Beijing 100049, Hefei 230026, People's Republic of China*

⁶⁰ *Sun Yat-Sen University, Guangzhou 510275, People's Republic of China*

⁶¹ *Suranaree University of Technology, University Avenue 111, Nakhon Ratchasima 30000, Thailand*

⁶² *Tsinghua University, Beijing 100084, People's Republic of China*

⁶³ *Turkish Accelerator Center Particle Factory Group, (A)Istinye University, 34010, Istanbul, Turkey; (B)Near East University, Nicosia, North Cyprus, 99138, Mersin 10, Turkey*

⁶⁴ *University of Bristol, H H Wills Physics Laboratory, Tyndall Avenue, Bristol, BS8 1TL, UK*

- ⁶⁵ *University of Chinese Academy of Sciences, Beijing 100049, People's Republic of China*
- ⁶⁶ *University of Groningen, NL-9747 AA Groningen, The Netherlands*
- ⁶⁷ *University of Hawaii, Honolulu, Hawaii 96822, USA*
- ⁶⁸ *University of Jinan, Jinan 250022, People's Republic of China*
- ⁶⁹ *University of Manchester, Oxford Road, Manchester, M13 9PL, United Kingdom*
- ⁷⁰ *University of Muenster, Wilhelm-Klemm-Strasse 9, 48149 Muenster, Germany*
- ⁷¹ *University of Oxford, Keble Road, Oxford OX13RH, United Kingdom*
- ⁷² *University of Science and Technology Liaoning, Anshan 114051, People's Republic of China*
- ⁷³ *University of Science and Technology of China, Hefei 230026, People's Republic of China*
- ⁷⁴ *University of South China, Hengyang 421001, People's Republic of China*
- ⁷⁵ *University of the Punjab, Lahore-54590, Pakistan*
- ⁷⁶ *University of Turin and INFN, (A)University of Turin, I-10125, Turin, Italy; (B)University of Eastern Piedmont, I-15121, Alessandria, Italy; (C)INFN, I-10125, Turin, Italy*
- ⁷⁷ *Uppsala University, Box 516, SE-75120 Uppsala, Sweden*
- ⁷⁸ *Wuhan University, Wuhan 430072, People's Republic of China*
- ⁷⁹ *Yantai University, Yantai 264005, People's Republic of China*
- ⁸⁰ *Yunnan University, Kunming 650500, People's Republic of China*
- ⁸¹ *Zhejiang University, Hangzhou 310027, People's Republic of China*
- ⁸² *Zhengzhou University, Zhengzhou 450001, People's Republic of China*
- ^a *Deceased*
- ^b *Also at the Moscow Institute of Physics and Technology, Moscow 141700, Russia*
- ^c *Also at the Novosibirsk State University, Novosibirsk, 630090, Russia*
- ^d *Also at the NRC "Kurchatov Institute", PNPI, 188300, Gatchina, Russia*
- ^e *Also at Goethe University Frankfurt, 60323 Frankfurt am Main, Germany*
- ^f *Also at Key Laboratory for Particle Physics, Astrophysics and Cosmology, Ministry of Education; Shanghai Key Laboratory for Particle Physics and Cosmology; Institute of Nuclear and Particle Physics, Shanghai 200240, People's Republic of China*
- ^g *Also at Key Laboratory of Nuclear Physics and Ion-beam Application (MOE) and Institute of Modern Physics, Fudan University, Shanghai 200443, People's Republic of China*
- ^h *Also at State Key Laboratory of Nuclear Physics and Technology, Peking University, Beijing*

100871, People's Republic of China

ⁱ Also at School of Physics and Electronics, Hunan University, Changsha 410082, China

^j Also at Guangdong Provincial Key Laboratory of Nuclear Science, Institute of Quantum Matter, South China Normal University, Guangzhou 510006, China

^k Also at MOE Frontiers Science Center for Rare Isotopes, Lanzhou University, Lanzhou 730000, People's Republic of China

^l Also at Lanzhou Center for Theoretical Physics, Lanzhou University, Lanzhou 730000, People's Republic of China

^m Also at the Department of Mathematical Sciences, IBA, Karachi 75270, Pakistan

ⁿ Also at Ecole Polytechnique Federale de Lausanne (EPFL), CH-1015 Lausanne, Switzerland

^o Also at Helmholtz Institute Mainz, Staudinger Weg 18, D-55099 Mainz, Germany

^p Also at Hangzhou Institute for Advanced Study, University of Chinese Academy of Sciences, Hangzhou 310024, China

Materials and Methods

BESIII experiment and simulation

The BESIII detector (26, 27) is designed to collect data from electron-positron collisions in the center-of-mass energy range from 1.84 to 4.95 GeV. The cylindrical core of the BESIII detector covers 93% of the full solid angle. The detector includes a helium-based multilayer drift chamber (MDC), providing measurements of the momentum and decay vertex position of particle. Charged particle identification is performed using information from the MDC and a plastic scintillator time-of-flight system.

Simulated data are used to optimize the event selection algorithm, estimate potential background types and levels, improve the signal-to-noise ratio of the final dataset, and accurately compute the normalization factors for the maximum likelihood fit. The simulation is performed using the GEANT4-based (28) BESIII Object Oriented Simulation Tool project (29), where Geant4 is responsible for describing the geometry of the BESIII detector, the transportation of particles within the detector, and their interactions with matter. The production of J/ψ and known decay processes

is simulated using the KKMC (30) model and the BesEvtGen (31) model, while Lundcharm (32,33) is responsible for simulating the unknown decay mods of J/ψ . To reduce discrepancies between experimental and simulated data, a control channel $J/\psi \rightarrow p\bar{p}\pi^+\pi^-$ is employed to estimate differences in the tracking efficiency for charged particles. The discrepancy serves as a correction factor to reweight events in the simulated data, thereby decreasing the systematic uncertainties related to the tracking efficiency. Additionally, the detection efficiency in the simulated data is corrected to account for discrepancies in the azimuthal angle distributions of protons and antiprotons.

Selection Criteria

The data sample used in this analysis is based on $(10.087 \pm 0.044) \times 10^9 J/\psi$ events collected by BESIII in 2009, 2012, and 2017-2019. The event selection process for the data sample is as follows: Λ and $\bar{\Lambda}$ are required to decay to the charged final states $p\pi^-$ and $\bar{p}\pi^+$, respectively. The main drift chamber from BESIII detector detects the trajectories of charged particles. Charged tracks detected in the MDC are required to be within a polar angle (θ) range of $|\cos\theta| < 0.93$, where θ is defined with respect to the z -axis, which is the symmetry axis of the MDC. Charged tracks with momentum greater than 0.5 GeV/c are regarded as proton candidates, while those with momentum below this threshold are considered candidates for pions. Subsequently, the Λ and $\bar{\Lambda}$ candidates are constructed by pairing oppositely charged protons and pions with a vertex reconstruction, which constrains the production position of $p\pi^-$ and $\bar{p}\pi^+$ to a common vertex. Due to the long intrinsic lifetime of Λ (10^{-10} s), the decay vertex of Λ is generally located far from the e^+e^- collision point. Therefore, by constraining the vertex fitting with $\chi^2_{\text{vtx}} < 200$ and requiring a distance greater than zero from the e^+e^- interaction point, background processes originating from the collision point, such as $J/\psi \rightarrow p\bar{p}\pi^+\pi^-$, $\Delta^{++}\bar{p}\pi^-$, $\bar{\Delta}^{++}p\pi^+$ and $\Delta^{++}\bar{\Delta}^{++}$, can be effectively suppressed. To further reduce the background contribution from non- Λ events such as $J/\psi \rightarrow p\bar{p}\pi^+\pi^-$, the mass of Λ is restricted to be between 1.111 GeV/ c^2 and 1.121 GeV/ c^2 . Finally, an energy-momentum conservation constraint is performed on the $p\bar{p}\pi^+\pi^-$ hypothesis, requiring the sum of the four-momentum of the final-state particles to equal the initial four-momentum of e^+e^- . The χ^2 of the energy-momentum conservation constraints is required to be less than 60. This effectively removes background sources such as $J/\psi \rightarrow \gamma\eta_c(\eta_c \rightarrow \Lambda\bar{\Lambda})$ and $J/\psi \rightarrow \gamma\Lambda\bar{\Lambda}$, where these background decay modes contain the same final-state decay products as the signal decay mode but with an

additional photon.

After applying all the event selection criteria described above, the final number of events in the data sample is 3049187, with an estimated background of 3801 ± 63 events, resulting in a purity of 99.9%. The number of non-peaking background events in the data is estimated using the sideband region of the two-dimensional invariant mass spectrum of $p\pi^-$ and $\bar{p}\pi^+$, with the lower and higher sideband regions defined as $m_{p\pi^-/\bar{p}\pi^+} \in [1.098, 1.107]$ GeV/c² and $m_{p\pi^-/\bar{p}\pi^+} \in [1.125, 1.134]$ GeV/c², respectively. The yields of different peaking background sources are estimated using separate exclusive Monte Carlo samples, which are subsequently normalized to the data sample based on their respective branching fractions.

Differential decay probability

The differential decay probability of the $e^+e^- \rightarrow J/\psi \rightarrow \Lambda\bar{\Lambda} \rightarrow p\pi^-\bar{p}\pi^+$ process is given as

$$\begin{aligned} \frac{d\sigma}{d\Omega} \propto \sum_{[\lambda], m, m'} \rho_{m, m'} d_{m, \lambda_\Lambda - \lambda_{\bar{\Lambda}}}^{j=1}(\theta_\Lambda) d_{m', \lambda'_\Lambda - \lambda'_{\bar{\Lambda}}}^{j=1}(\theta_\Lambda) \mathcal{M}_{\lambda_\Lambda, \lambda_{\bar{\Lambda}}} \mathcal{M}_{\lambda'_\Lambda, \lambda'_{\bar{\Lambda}}}^* \delta_{m, m'} \\ \times D_{\lambda_\Lambda, \lambda_p}^{*j=1/2}(\phi_p, \theta_p) D_{\lambda'_\Lambda, \lambda'_p}^{j=1/2}(\phi_p, \theta_p) \mathcal{H}_{\lambda_p} \mathcal{H}_{\lambda'_p}^* \\ \times D_{\lambda_{\bar{\Lambda}}, \lambda_{\bar{p}}}^{*j=1/2}(\phi_{\bar{p}}, \theta_{\bar{p}}) D_{\lambda'_{\bar{\Lambda}}, \lambda'_{\bar{p}}}^{j=1/2}(\phi_{\bar{p}}, \theta_{\bar{p}}) \bar{\mathcal{H}}_{\lambda_{\bar{p}}} \bar{\mathcal{H}}_{\lambda'_{\bar{p}}}^*, \end{aligned} \quad (\text{S1})$$

where $[\lambda]$ is a set of all possible indexes representing the helicities of Λ and $\bar{\Lambda}$ via the J/ψ resonance and the helicities of p and \bar{p} via Λ and $\bar{\Lambda}$, respectively. The direction of the Λ in the J/ψ rest frame, along with the motion directions of the proton (p) and antiproton (\bar{p}) in the rest frames of the Λ and $\bar{\Lambda}$, respectively, are described by the kinematic variable $\xi = (\theta_\Lambda, \theta_p, \theta_{\bar{p}}, \phi_p, \phi_{\bar{p}})$. The definition of the corresponding coordinate system, shown in Fig. S1, is as follows: In the rest frame of the Λ hyperon, the Cartesian coordinate system $(X_\Lambda, Y_\Lambda, Z_\Lambda)$ is defined, with the unit vector Z_Λ aligned with the momentum direction of Λ in the center-of-mass frame for e^+e^- . The unit vectors Y_Λ and X_Λ are defined as $Y_\Lambda = Z \times Z_\Lambda$ and $X_\Lambda = Y_\Lambda \times Z_\Lambda$, respectively. For the $\bar{\Lambda}$, the coordinate system $(X_{\bar{\Lambda}}, Y_{\bar{\Lambda}}, Z_{\bar{\Lambda}})$ is constructed as $(-X_\Lambda, Y_\Lambda, -Z_\Lambda)$. The motion directions of the proton p and antiproton \bar{p} are characterized by the angles $(\theta_p, \theta_{\bar{p}}, \phi_p, \phi_{\bar{p}})$ in their separate systems.

The amplitude for the $J/\psi \rightarrow \Lambda\bar{\Lambda}$ decay is written as (14)

$$\mathcal{M}_{\lambda_\Lambda, \lambda_{\bar{\Lambda}}} = \epsilon_\mu (\lambda_\Lambda - \lambda_{\bar{\Lambda}}) \bar{u}(\lambda_\Lambda, p_\Lambda) (F_V \gamma^\mu + \frac{i}{2m_\Lambda} \sigma^{\mu\nu} q_\nu H_\sigma + \gamma^\mu \gamma^5 F_A + \sigma^{\mu\nu} \gamma^5 q_\nu H_T) v(\lambda_{\bar{\Lambda}}, p_{\bar{\Lambda}}), \quad (\text{S2})$$

where m_Λ is Λ hyperon mass, and p_Λ and $p_{\bar{\Lambda}}$ are the four momenta of Λ and $\bar{\Lambda}$, respectively. The form factors F_V and H_σ are related to the electric and magnetic form factors G_2 and G_1 (14), with $F_V = G_1 - 4m_\Lambda^2 \frac{(G_1 - G_2)}{(p_1 - p_2)^2}$ and $H_\sigma = 4m_\Lambda^2 \frac{(G_1 - G_2)}{(p_1 - p_2)^2}$. Two parameters, $\alpha_{J/\psi} = \frac{m_{J/\psi}^2 |G_1|^2 - 4m_\Lambda^2 |G_2|^2}{m_{J/\psi}^2 |G_1|^2 + 4m_\Lambda^2 |G_2|^2}$ and $\frac{G_1}{G_2} = \left| \frac{G_1}{G_2} \right| e^{-i\Delta\Phi}$, are subsequently introduced to characterize the polarization of Λ (34, 35). The form factor $G_1 = (161 \pm 4) \times 10^{-5}$, determined from the measured decay rate of $J/\psi \rightarrow \Lambda \bar{\Lambda}$ and $\alpha_{J/\psi}$ (15, 36), is taken as a real parameter. The helicity amplitude \mathcal{H}_{λ_i} contains the dynamics of the weak decay $\Lambda \rightarrow p\pi$. It is used to define the parity-violating parameter α_Λ , allowing for the construction of the CP-violating observable A_{CP} , the relative difference between Λ and $\bar{\Lambda}$ decays (37). A non-zero transverse polarization of Λ , along with the most precise test of CP symmetry conservation in Λ decay, has recently been measured at BESIII (35).

Maximum log-likelihood fit procedure

A maximum likelihood fit is performed on the data based on the angular distribution defined as:

$$\mathcal{L} = \prod_{i=1}^N \mathcal{P}(\xi^i; \vec{\lambda}) = \prod_{i=1}^N C \mathcal{W}(\xi^i; \vec{\lambda}) \epsilon(\xi^i). \quad (\text{S3})$$

Here, $\mathcal{P}(\xi^i; \vec{\lambda})$ is the probability density function where the set of helicity angles $\xi^i = (\theta_\Lambda^i, \theta_p^i, \theta_{\bar{p}}^i, \phi_p^i, \phi_{\bar{p}}^i)$ denotes the event i , and $\vec{\lambda} = (P_L, G_2, F_A, H_T, \alpha_\Lambda, \alpha_{\bar{\Lambda}})$ represents the fitted parameters. The joint angular distribution $\mathcal{W}(\xi^i; \vec{\lambda}) \propto \frac{d\sigma}{d\Omega}$ is defined in Equation S1. The detection efficiency is denoted by $\epsilon(\xi^i)$. The normalization factor $C^{-1} = \frac{1}{N_{\text{MC}}} \sum_{j=1}^{N'} \mathcal{W}(\xi^j; \vec{\lambda}) \epsilon(\xi^j)$ is estimated using a simulated sample of N' events generated uniformly in the phase space, selected based on the same event criteria as in the data analysis. Simulated data are generated at approximately 100 times the size of the accepted data to improve the accuracy of the normalization factor. The RooFit package (20) is applied to determine the fitted parameter, with the objective function defined as:

$$S = -\ln \mathcal{L}_{\text{data}} + \ln \mathcal{L}_{\text{bg}}, \quad (\text{S4})$$

where $\mathcal{L}_{\text{data}}$ and \mathcal{L}_{bg} are the likelihood values for the data and the background events, respectively. The fit results are presented in Table 1, where parameters dependent on combinations of fitted parameters account for their correlations. The correlation coefficients among the fitted parameters are listed in Table S2.

Systematic uncertainties

The systematic uncertainties in this measurement arise from various sources, including background estimation, charged particle reconstruction, vertex reconstruction for $\Lambda(\bar{\Lambda})$, energy-momentum conservation constraints, detector resolution, and the values of the parameters G_1 , $m_{J/\psi}$, m_Z , and g_V . Systematic effects related to charged particle reconstruction, vertex reconstruction, and energy-momentum conservation constraints are investigated using data-driven methods with different control samples to quantify the discrepancies between experimental and simulated data. Table S1 provides a summary of the absolute systematic uncertainties from each source. The total systematic uncertainty for each fitting parameter is obtained by combining the individual contributions in quadrature.

1. **Background estimation.** The systematic uncertainties associated with the background originate from uncertainties in estimating the number of background events. To evaluate this effect, the number of background events is varied by one standard deviation in the joint maximum-likelihood fit. The resulting deviation in the fitted parameters is taken as the systematic uncertainty. Studies show that the impact of this uncertainty on the fitting parameters is negligible.
2. **Charged particle reconstruction.** The systematic uncertainty from the reconstruction efficiency of charged particles is studied using the control sample $J/\psi \rightarrow p\bar{p}\pi^+\pi^-$. This sample is used to evaluate the discrepancy in track reconstruction efficiency for charged particles (p, \bar{p}, π^+, π^-) in the MDC between experimental and simulated data. It is assumed that the tracking efficiency depends only on the polar angle θ and transverse momentum P_T of the charged particles. To account for this, the reconstruction efficiencies in the simulated data are adjusted event by event to match those observed in the experimental data. The systematic uncertainty in charged particle reconstruction arises from statistical fluctuations in the efficiency correction factor applied to the simulated data. To quantify this uncertainty, the correction factor's central value is sampled from a Gaussian distribution, incorporating its statistical uncertainty. This procedure is repeated 100 times, generating 100 sets of simulated data with varying correction factors for the maximum likelihood fit. The resulting 100 sets of fit results form a distribution, whose standard deviation is taken as the systematic uncertainty.

This uncertainty was found to be negligible.

3. **Λ and $\bar{\Lambda}$ vertex reconstruction.** The systematic uncertainty from the efficiency of the Λ and $\bar{\Lambda}$ vertex reconstruction is evaluated using the control sample $J/\psi \rightarrow \Lambda\bar{\Lambda}, \Lambda(\bar{\Lambda}) \rightarrow p\pi^-(\bar{p}\pi^+)$. The angular distribution of the final-state particles $p\bar{p}\pi^+\pi^-$ is divided into different regions to examine discrepancies in vertex reconstruction efficiency between experimental and simulated data within each bin. The vertex reconstruction efficiency in the simulated data is then adjusted to match that of the experimental data. Following the methodology used for charged particle reconstruction uncertainties, this correction is applied 100 times to generate 100 sets of simulated data with varying correction factors for the fitting. The systematic uncertainty for each parameter is determined as the difference between the central values of these 100 fits and the measured results.
4. **Energy-momentum conservation constraints.** The systematic uncertainty arising from the efficiency of the energy-momentum conservation constraints is evaluated using the control sample $J/\psi \rightarrow \Lambda\bar{\Lambda}, \Lambda(\bar{\Lambda}) \rightarrow p\pi^-(\bar{p}\pi^+)$. The angular distribution of the final-state particles $p\bar{p}\pi^+\pi^-$ in the control sample is divided into distinct regions to examine variations in the energy-momentum conservation constraints efficiency between the experimental and the simulated samples. The efficiency in the simulated data is then corrected to match that of the experimental data. Following a procedure similar to that used for charged particle reconstruction uncertainties, this correction is iterated 100 times to generate 100 sets of simulated data with varying correction factors for the fit. The standard deviation of the distribution of these 100 fitting results is taken as the systematic uncertainty.
5. **Detector resolution.** To assess the impact of detector resolution, we generated 10 sets of simulated data, each with the same size as the experimental data. These datasets were sampled according to the angular distribution in Equation S1, with input parameters fixed to the measured value obtained from the experimental data. The samples were reconstructed using the same event selection criteria as applied to the experimental data. After fitting the ten sets of simulated data, the differences between the central values of the fitting results and the input values were taken as the systematic uncertainty.

6. **The value of G_1 .** Since all form factors were normalized to G_1 during the maximum likelihood fit, the final fitting results of these form factors are influenced by the magnitude of G_1 . Given that $G_1 = (161 \pm 4) \times 10^{-5}$, the relative systematic uncertainty introduced by these form factors is estimated to be 2.5%.

7. **The value of $m_{J/\psi}$, m_Z and g_V .** The input values of $m_{J/\psi}$ and m_Z are required to calculate $\sin^2 \theta_W$. According to the latest results from (36), the relative systematic uncertainty introduced by $m_{J/\psi}$ and m_Z on $\sin^2 \theta_W$ is estimated to be 0.2%, which is negligible. Additionally, the relative systematic uncertainty introduced by g_V on $\text{Re}(d_\Lambda)$ and $\text{Im}(d_\Lambda)$ is estimated to be 0.9%, which is also negligible.

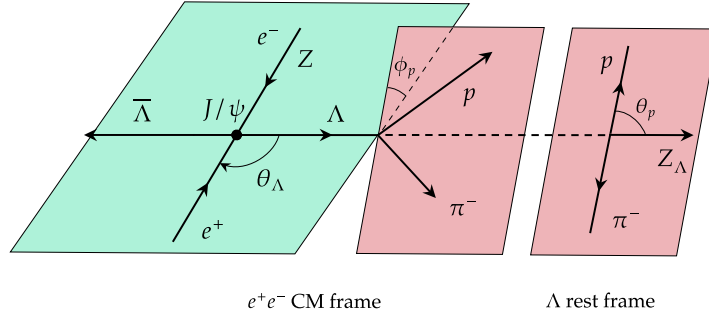


Figure S1: Definition of the Cartesian coordinate system for the $e^+e^- \rightarrow J/\psi \rightarrow \Lambda \bar{\Lambda}$ with $\Lambda(\bar{\Lambda}) \rightarrow p\pi^- (\bar{p}\pi^+)$. In the rest frame of Λ , the coordinate system $(X_\Lambda, Y_\Lambda, Z_\Lambda)$ is defined with Z_Λ aligned along the momentum direction of Λ in the e^+e^- center-of-mass frame. The other unit vectors are defined as $Y_\Lambda = Z \times Z_\Lambda$ and $X_\Lambda = Y_\Lambda \times Z_\Lambda$, in which Z denotes the momentum direction of the electron beam in the e^+e^- center-of-mass frame. For the $\bar{\Lambda}$, the coordinate system $(X_{\bar{\Lambda}}, Y_{\bar{\Lambda}}, Z_{\bar{\Lambda}})$ is constructed as $(-X_\Lambda, Y_\Lambda, -Z_\Lambda)$.

Table S1: Absolute systematic uncertainties on the fitted parameters.

Source	$\Lambda/\bar{\Lambda}$ vertex fit	Kinematic fit	Detector resolution	G_1 value	Total
$\alpha_\Lambda(10^{-3})$	0.1	0.4	0.7	-	0.8
$\alpha_{\bar{\Lambda}}(10^{-3})$	0.1	0.2	0.8	-	0.8
$Re(G_2)(10^{-6})$	0.9	0.3	1.0	24	24
$Im(G_2)(10^{-6})$	0.2	0.2	3.0	23	23
$P_L(10^{-3})$	0.2	0.1	0.8	-	0.8
$Re(F_A)(10^{-6})$	0.3	0.2	3.1	0.1	3.1
$Im(F_A)(10^{-6})$	0.1	0.4	2.5	0.2	2.5
$Re(H_T)(10^{-6} \text{ GeV}^{-1})$	0.1	0.1	0.1	0.0	0.2
$Im(H_T)(10^{-6} \text{ GeV}^{-1})$	0.2	0.1	0.3	0.0	0.4
$\alpha_{J/\psi}(10^{-3})$	0.5	0.0	1.6	-	1.7
$\Delta\phi(10^{-3})$	0.4	0.3	1.2	-	1.3
$A_{CP}(10^{-3})$	0.0	0.1	1.0	-	1.1
$\sin^2\theta_W(10^{-1})$	0.1	0.0	2.6	-	2.6
$Re(d_\Lambda)(10^{-19} \text{ e cm})$	0.3	0.3	0.2	0.1	0.5
$Im(d_\Lambda)(10^{-19} \text{ e cm})$	0.3	0.2	0.5	0.1	0.6

Table S2: Correlation matrix of the fitted parameters.

Paras.	$Im(F_A)$	$Im(H_T)$	$Im(G_2)$	P_L	$Re(F_A)$	$Re(H_T)$	$Re(G_2)$	α_Λ	$\alpha_{\bar{\Lambda}}$
$Im(F_A)$	1.000	0.001	0.033	-0.002	-0.085	-0.000	0.057	0.013	-0.010
$Im(H_T)$		1.000	0.001	-0.012	-0.003	0.351	-0.003	-0.046	-0.045
$Im(G_2)$			1.000	-0.002	-0.045	0.002	-0.407	-0.034	0.049
P_L				1.000	-0.000	-0.029	0.007	0.023	0.019
$Re(F_A)$					1.000	0.003	-0.139	-0.002	-0.008
$Re(H_T)$						1.000	0.003	-0.039	-0.038
$Re(G_2)$							1.000	0.097	-0.100
α_Λ								1.000	0.848
$\alpha_{\bar{\Lambda}}$									1.000